Photonic Refrigeration from Time-Modulated Thermal Emission

Siddharth Buddhiraju, Wei Li, and Shanhui Fan

Photonic refrigeration from time-modulated thermal emission

Siddharth Buddhiraju, Wei Li, and Shanhui Fan*

Ginzton Laboratory, Department of Electrical Engineering, Stanford University, Stanford, CA

(Dated: January 17, 2020)

We develop theoretical and computational formalisms to describe thermal radiation from temporally modulated systems. We show that such a modulation results in a photon-based active cooling mechanism. This mechanism has a high thermodynamic performance that can approach the Carnot limit. Our work points to exciting new avenues in active, time-modulated control of thermal emission for cooling and energy harvesting applications.

Thermal radiation is a fundamental aspect of nature that is of central importance to energy technology. Recent advances in sub-wavelength nanophotonic structures have offered new possibilities for controlling thermal radiation [1–8] and enabled new applications such as passive radiative cooling [4]. However, almost all existing works on thermal radiation control have focused on passive systems, where heat can only flow from a high-temperature to a low-temperature object, in accordance with the second law of thermodynamics. Recently, Latella et al. [9] considered radiative thermal exchange between two bodies, where the temperature of at least one body is oscillating in time. They observe a radiative shuttling effect, where there can be a net heat flow when the two bodies have the same time-averaged temperature. However, in their system, the bodies are in thermal equilibrium at any given time and the instantaneous heat flow is always from the hotter to the colder body.

In this Letter, we consider thermal emission from systems whose refractive index undergoes temporal modulation. In recent years, such index modulation has offered exciting opportunities to manipulate photons, such as optical isolation [10–12] and the breaking of symmetry between emission and absorption [13]. While time-modulated systems such as electro-optic modulators have been widely used in optical information processing, the thermodynamic implications of such modulation have not been previously explored. In this work, we develop a statistical-temporal coupled-mode theory to show that temporal refractive-index modulation of a thermal photonic system can be used to pump heat from a low-temperature to a high-temperature reservoir, realizing a purely photon-based refrigeration mechanism. Further, by a rigorous fluctuational electrodynamics approach, we verify the predictions of our theory and numerically demonstrate photonic refrigeration by computing the heat transfer from a time-modulated structure at a certain temperature to a passive thermal emitter at a higher temperature. Our work points to exciting new avenues in active, time-modulated control of thermal emission for cooling and energy conversion applications.
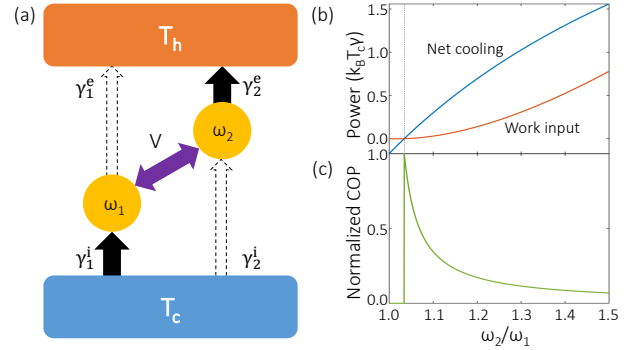

FIG. 1. (a) General setup of a thermal photonic refrigerator operating between a cold side at T_c and a hot side T_h by coupling two modes at frequencies $\omega_{1,2}$ using time-modulation (purple arrow). (b) Net cooling power (blue curve) and work input (red curve) normalized to $k_B T_c \gamma$, as a function of the ratio of the frequencies of the two modes for $T_h = 300$ K and $T_c = 290$ K at $V = 2\gamma$. (c) Coefficient of performance (COP) of the refrigerator normalized to the Carnot bound.

Consider a cavity with modes 1 and 2 at frequencies $\omega_{1,2}$, respectively, with $\omega_1 < \omega_2$, as shown schematically in Fig. 1(a). The amplitudes in the two modes $a_{1,2}$ are normalized such that $|a_{1,2}|^2$ represent the energy in the modes. The modes have internal loss rates $\gamma^i_{1,2}$ due to absorption and are in thermal equilibrium with a heat bath at temperature T_c. The modes also radiatively couple to an external heat bath at temperature $T_h (\geq T_c)$ via coupling rates $\gamma^e_{1,2}$. By the fluctuation-dissipation theorem, there are associated compensating noise sources [14, 15] $n^i_{1,2}$ for internal loss and $n^e_{1,2}$ for external radiative coupling, respectively. The strength of these noise sources are defined by $\langle n^{i*}_{1,2}(\omega) n^i_{1,2}(\omega') \rangle = 2\pi \delta(\omega - \omega') \Theta(\omega, T_c)$ and $\langle n^{e*}_{1,2}(\omega) n^e_{1,2}(\omega') \rangle = 2\pi \delta(\omega - \omega') \Theta(\omega, T_h)$, where $\langle \cdot \rangle$ denotes a thermal ensemble average and $\Theta(\omega, T) = \hbar\omega/(\exp(\hbar\omega/k_B T) - 1)$ is the Planck distribution at frequency ω and temperature T. Defining $\mathbf{a} = (a_1, a_2)^T$, $\mathbf{n}_i = (n^i_1, n^i_2)^T$ and $\mathbf{n}_e = (n^e_1, n^e_2)^T$, the time evolution of the two modes is described by

$$-i\frac{d}{dt}\mathbf{a} = (H_0 - i\Gamma_i - i\Gamma_e + M(t))\,\mathbf{a} + D_i\mathbf{n}_i + D_e\mathbf{n}_e.$$

(1)

Here, $H_0 = \text{diag}(\omega_1, \omega_2)$ is the Hamiltonian of the unmodulated, closed system. $D_i = \text{diag}(\sqrt{2\gamma_1^i}, \sqrt{2\gamma_2^i})$, $D_e = \text{diag}(\sqrt{2\gamma_1^e}, \sqrt{2\gamma_2^e})$, $\Gamma_i = D_i D_i^\dagger / 2$ and $\Gamma_e = D_e D_e^\dagger / 2$. The operator $M(t)$ describes the modulation-induced coupling between the modes. Here, we assume that the cavity is modulated by an index modulation proportional to $\cos(\Omega t)$, where $\Omega = \omega_2 - \omega_1$. We assume that the reservoirs are sufficiently large such that their temperatures are not affected by the modulation. In order words, the modulation as well as the interaction between the modes and the reservoirs are much faster than the inverse time constants of the reservoirs themselves. Under the rotating-wave approximation, $M(t)$ is given by (see Supplementary Information (SI), Section I)

$$M(t) = \begin{pmatrix} 0 & \sqrt{\frac{\omega_1}{\omega_2}} V e^{-i\Omega t} \\ \sqrt{\frac{\omega_2}{\omega_1}} V^* e^{i\Omega t} & 0 \end{pmatrix}, \qquad (2)$$

where V is related to the strength of the index modulation. Note that $M(t)$ is *not* Hermitian since the modal amplitudes $a_{1,2}(t)$ are normalized with respect to energy, and such time-modulation preserves the total number of photons [10, 11] but not the total energy.

We now show that the system shown in Fig. 1(a), which is described by Eqs. (1)-(2), can achieve photonic refrigeration. For illustration, we first consider the simplest case: in the setup of Fig. 1(a), we assume that mode 1 has no radiative coupling to the high-temperature heat bath, i.e., $\gamma_1^e = 0$ (dotted arrow). Mode 2 is assumed to have a nonzero external radiative coupling rate, but no internal loss, i.e., $\gamma_2^i = 0$ (dotted arrow). Therefore, the thermal emission and absorption of the unmodulated system in this ideal limit is zero. For simplicity, we take the remaining rates to be $\gamma_1^i = \gamma_2^e = \gamma$ (solid arrows). For this ideal system, the flux of the thermal emission from the cold side in the presence of modulation is (see SI Sec. IV, based on Secs. II-III)

$$P_{out} = 4\gamma^2 |V|^2 \frac{\omega_2}{\omega_1} \int d\omega \frac{1}{|Z_2(\omega)|^2} \Theta(\omega - \Omega, T_c), \quad (3)$$

while the flux received from the hot side at T_h is

$$P_{in} = 4\gamma^2 |V|^2 \int d\omega \frac{1}{|Z_1(\omega)|^2} \Theta(\omega + \Omega, T_h), \quad (4)$$

for a work input of

$$\dot{W} = 4\gamma^2 |V|^2 \int d\omega \left[\frac{\Omega}{\omega_1} \frac{\Theta(\omega, T_c)}{|Z_1(\omega)|^2} - \frac{\Omega}{\omega_2} \frac{\Theta(\omega, T_h)}{|Z_2(\omega)|^2} \right], \quad (5)$$

where $Z_{1,2}(\omega) = (\omega - \omega_{1,2} - i\gamma)^2 - |V|^2$. As seen from Eqs. (3)-(5), when the modulation is turned on, i.e., $V \neq 0$, a fraction of the thermally generated photons from mode 1 are up-converted to mode 2 and emitted. These photons carry power P_{out} away from the low-temperature

reservoir and constitute a cooling mechanism. Similarly, a fraction of the photons received by mode 2 are down-converted to mode 1 and absorbed. These photons carry power P_{in} into the low-temperature heat bath and constitute a heating mechanism. In Fig. 1(b), we plot the net cooling given by $P_{out} - P_{in} - \dot{W}$ (blue curve) and the work input $\dot{W}$ (red curve) as a function of the ratio ω_2/ω_1 for $V = 2\gamma$. Net cooling starts to occur when

$$\frac{\omega_2}{\omega_1} \geq \frac{T_h}{T_c}. \qquad (6)$$

As ω_2/ω_1 increases beyond the threshold value of T_h/T_c, the cooling power also increases. In Fig. 1(c), we plot the coefficient of performance (COP), defined as the ratio between the cooling power and the work input, as a function of ω_2/ω_1. We observe that the COP reaches the Carnot bound of $T_c/(T_h - T_c)$ at the threshold condition of Eq. (6), and decreases as ω_2/ω_1 increases beyond the threshold.

The threshold condition for ω_2/ω_1 in Eq. (6) can be derived analytically from Eqs.(3)-(5) (SI Section IV). Here, we provide an intuitive argument. For simplicity, we assume the classical limit of $k_B T_{c,h} \gg \hbar\omega_{1,2}$. In the unmodulated cavity, the number of thermal photons in mode 1 is $k_B T_c / \hbar\omega_1$, while that in mode 2 is $k_B T_h / \hbar\omega_2$ due to its radiative coupling to the high-temperature heat bath and lack of internal loss. When modulation is turned on, since the rate of up- and down-conversion for an individual photon is equal [10, 11], net cooling will be observed when $k_B T_c / \hbar\omega_1 \geq k_B T_h / \hbar\omega_2$, leading to the threshold condition of Eq. (6). When the condition of Eq. (6) is met, for each photon emitted by the modulated system, the system at T_c experiences cooling by $\hbar\omega_1$. The work input per emitted photon is the energy difference of the two modes, $\hbar\omega_2 - \hbar\omega_1$. Therefore, the COP is given by

$$COP = \frac{\omega_1}{\omega_2 - \omega_1} \leq \frac{T_c}{T_h - T_c}, \qquad (7)$$

where the inequality follows from Eq. (6). This upper bound indicates that modulation-induced refrigeration obeys the Carnot limit on performance. Interestingly, the value of COP for this ideal refrigerator is independent of the modulation strength V. A rigorous derivation of the Carnot bound on the COP is included in the SI (Section V).

Motivated by the theoretical results above, we consider a physical structure shown in Fig. 2(a). The structure consists of a one-dimensional photonic crystal comprising two materials with dielectric constants $\epsilon_1 = 14$ (blue layers) and $\epsilon_2 = 4$ (yellow layers) each 1 μm thick, resulting in a band gap. We introduce two modes in the band gap using two defect layers with thicknesses 2.1
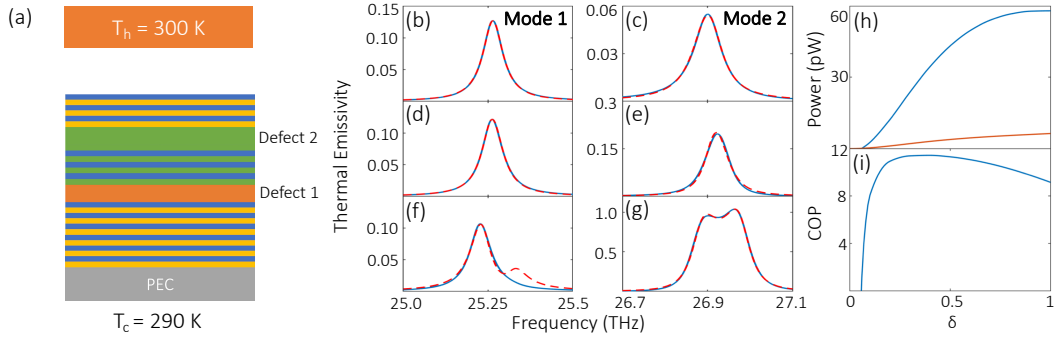
FIG. 2. (a) Physical structure to demonstrate cooling induced by modulation. All parameters in the main text. Calculated emission spectrum of the two modes in the structure (solid blue lines) superimposed by a coupled mode theory fit (red dotted lines) for (b)-(c) the unmodulated structure, (d)-(e) for $\delta = 0.1$ and (f)-(g) for $\delta = 0.5$. Modulation frequency $\Omega = 2\pi \cdot 1.64$ THz. (h) Net cooling of the cold side (blue) and work input (red) to the modulated layers for the single channel, as a function of the modulation strength δ. (i) The corresponding COP. The COP approaches a value of 5.18 for large δ.

μm and 1.6 μm, respectively, indicated by 'Defect 1' and 'Defect 2' in Fig. 2(a). The material constituting the Defect 1 (orange layer) is assumed to be a narrowband absorber. Such narrowband absorbers help suppress parasitic heating arising from frequencies away from the modes under consideration. We assume Defect 1 comprises a medium that is a random mixing of silicon carbide and a lossless high-index medium of $\epsilon_1 = 14$ in a 1:9 ratio. Using the Maxwell-Garnett approximation, the dielectric constant of such a medium is then $\epsilon(\omega) = 0.1 \times \epsilon_\infty(\omega_{LO}^2 - \omega^2 - i\omega\gamma)/(\omega_{TO}^2 - \omega^2 - i\omega\gamma) + 0.9 \times 14$, where $\epsilon_\infty = 6.7$, $\omega_{LO} = 1.83 \times 10^{14}$ rad/s, $\omega_{TO} = 1.49 \times 10^{14}$ rad/s and $\gamma = 8.97 \times 10^{11}$ rad/s [16]. The layers in between the defects, marked in green, experience a temporal modulation given by $\epsilon(t) = \epsilon_2 + \delta \cos(\Omega t)$ while Defect 2 undergoes a similar modulation of $\epsilon(t) = \epsilon_1 + \delta \cos(\Omega t)$, where δ is the modulation strength and Ω is the modulation frequency. The structure here involves modulation over alternating layers since it was observed that such modulation produces the highest performance; however, modulating all or a subset of layers between the two defects also produces a comparable cooling power. This structure is maintained at $T_c = 290$ K and faces a narrowband emitter in the far-field, composed of the same material as Defect 1 and at a temperature of $T_h = 300$ K.

To perform calculations of thermal emission and absorption, we extend the formalism of radiative heat transfer [17, 18] to include time-varying dielectric functions. This formalism combines rigorous coupled wave analysis [19, 20] with the fluctuation-dissipation theorem [18, 21] to compute thermal emission from spatiotemporally modulated layered structures. Within this formalism, the net heat transfer between two bodies at temperatures T_h and T_c separated by a vacuum gap is given by

$$\Delta P = \int_0^\infty d\omega \int_{-\infty}^\infty \frac{dk_x}{2\pi} \int_{-\infty}^\infty \frac{dk_y}{2\pi} \Big[\Phi_f(\omega, k_x, k_y) \times$$
$$\Theta(\omega, T_c) - \Phi_b(\omega, -k_x, -k_y)\Theta(\omega, T_h) \Big], \quad (8)$$

where (k_x, k_y) are the wavevector components parallel to the layers and $\Phi_{f,b}(\omega, k_x, k_y)$ are the Poynting flux spectra in the vacuum gap generated by sources in the cold and hot sides, respectively. For passive reciprocal structures, $\Phi_f(\omega, k_x, k_y) = \Phi_b(\omega, -k_x, -k_y)$. In this system, $\Phi_f(\omega, k_x, k_y) \neq \Phi_b(\omega, -k_x, -k_y)$ due to the presence of an actively modulated region. In addition to the flux of thermally generated photons, we compute the work done by the modulation directly from Maxwell's equations, given by (see SI, Section VI)

$$\dot{W} = \int_0^\infty d\omega \frac{2}{\pi} \omega \Theta(\omega, T) \int d\mathbf{r} \int d\mathbf{r}' \, \mathrm{Im} \, \mathrm{Tr} \big[\mathcal{W}\hat{\epsilon}(\mathbf{r}) \times$$
$$\mathcal{G}(\mathbf{r}, \mathbf{r}')\delta_{\omega,\omega'} \, \mathrm{Im} \left[\epsilon(\mathbf{r}') \right] \mathcal{G}^\dagger(\mathbf{r}, \mathbf{r}') \big], \quad (9)$$

where $\mathcal{W}$, $\delta_{\omega,\omega'}$ and $\hat{\epsilon}$ are matrices defined by $\mathcal{W}_{nm} = (\omega + m\Omega)\delta_{nm}$, $\delta_{\omega,\omega'} = \delta_{n=0,m=0}$ and $\hat{\epsilon}_{nm}(\mathbf{r}) = \frac{\Omega}{2\pi} \int_0^{2\pi/\Omega} \epsilon(\mathbf{r}, t) e^{-i(n-m)\Omega t} dt$, with $\hat{\epsilon}^\dagger = \hat{\epsilon}$ in the modulation layer. $\mathcal{G}(\mathbf{r}, \mathbf{r}')$ is the Green's function for the electric field at $\mathbf{r}$ in the modulated layer originating from a source at $\mathbf{r}'$ in the lossy layers. The operator $\delta_{\omega,\omega'}$ ensures that thermal photons are generated only at ω but not at the sideband frequencies, since the lossy layer at $\mathbf{r}'$ is unmodulated. We also note that the expression for work in Eq. (5) is a coupled-mode theory version of the general formula given by Eq. (9).

As a first numerical demonstration, we fit our coupled-mode theory to direct numerical calculations of thermal emission into vacuum, for the structure shown in Fig. 2(a) without the hot side. In Fig. 2(b)-(c), we plot in

blue the emissivity of the two modes in the unmodulated structure in the $(k_x, k_y) = (0, 0)$ channel. We extract the parameters $\omega_{1,2}$, $\gamma^i_{1,2}$ and $\gamma^e_{1,2}$ by fitting the emissivity profiles, shown in red dotted lines (parameter values in SI, Section VII). In this structure, the lossy Defect 1 layer is further away from the top surface as compared to the lossless Defect 2 layer. Thus, γ^e_1 and γ^i_2 are much smaller than the other two rates and the thermal emission of the unmodulated system is very low. We introduce a modulation of $\delta \cos(\Omega t)$ in the green layers in Fig. 2(a), where $\delta = 0.1$ and $\Omega = \omega_2 - \omega_1 = 2\pi \cdot 1.64$ THz. Modulation at such a frequency can be achieved using a $\chi^{(2)}$ nonlinear process with a pump wave at the terahertz frequency. Such a modulation does not in principle generate loss or heat in the material being modulated. See also Ref. [22] for a recent work on four-wave mixing for near-field refrigeration. In Fig. 2(d)-(e), we plot the emissivities of the two modes from the numerical calculation in blue lines and fit them using our coupled-mode theory in red dotted lines, exhibiting a very good agreement. With modulation, the emissivity near ω_2 is dramatically enhanced compared to the unmodulated system. In fact, for a larger modulation of $\delta = 0.5$, shown in Fig. 2(f)-(g), the emission near ω_2 becomes super-Planckian: the emissivity, which is defined as the emitted power density normalized against a blackbody at the same temperature, begins to exceed unity. The results here demonstrate that there is significant up-conversion induced by the temporal modulation. In addition, we observe modulation-induced Rabi splitting [23] of the modes for $\delta = 0.5$, resulting in dips in thermal emission near the frequencies where emission was maximum in the unmodulated system.

To demonstrate cooling for this single channel, in the presence of the narrowband emitter on the hot side, in Fig. 2(h), we plot the net cooling of the cold side (blue curve) and the work input to the modulated region (red curve) as a function of the modulation strength δ. In Fig. 2(g), we plot the corresponding COP. It is seen that the system of Fig. 2(a) does achieve cooling for the single channel with a large COP, reaching a maximum value of about 11. For reference, the Carnot limit on performance for the temperatures used in our setup is $T_c/(T_h - T_c) = 29$, although this limit is attained only at net zero cooling power.

Now, we show that the system of Fig. 2(a) exhibits refrigeration even after integration over all propagating channels (k_x, k_y) in Eq. (8) and all frequencies. Defining $\Phi_{f,b}(\omega) = \int \int_{-\infty}^{\infty} dk_x dk_y \Phi_{f,b}(\omega, k_x, k_y)/4\pi^2$, in Fig. 3(a), we plot the spectral heat flux $\Phi_f(\omega)\Theta(\omega, T)$ (blue curve) and $\Phi_b(\omega)\Theta(\omega, T)$ (red curve) for the passive, unmodulated structure when the two sides are at the same temperature of 300 K. It is seen that $\Phi_f(\omega) = \Phi_b(\omega)$, as dictated by electromagnetic reciprocity. On the other
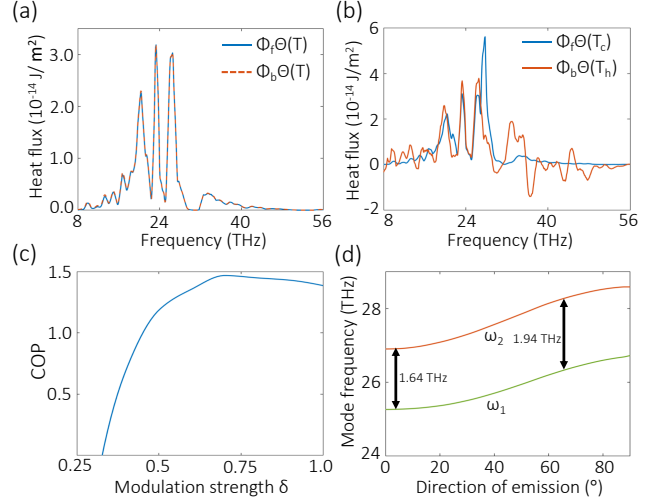

FIG. 3. Spectral heat flux in both forward (blue) and reverse (red) directions in for the structure of Fig. 2 for (a) the unmodulated structure at $T_h = T_c = 300K$ and (b) for $\delta = 0.5$, $T_c = 290$ K and $T_h = 300$ K. In (a), the two curves overlay perfectly over each other due to the absence of modulation. (c) COP of the modulated structure as a function of modulation strength δ. (d) Variation in the resonant frequencies of the two resonant modes in the structure of Fig. 2(a) as a function of the emission direction.

hand, in the presence of modulation, $\Phi_f(\omega) \neq \Phi_b(\omega)$ due to the active region on the cold side, where power is either consumed or generated. This is seen in Fig. 3(b) for a modulation of $\delta = 0.5$ and $\Omega = 2\pi \cdot 1.64$ THz, where $\Phi_f(\omega)\Theta(\omega, T_c)$ and $\Phi_b(\omega)\Theta(\omega, T_h)$ differ significantly in their spectral shape. Strikingly different from passive structures, $\Phi_b(\omega)$ can be negative at some frequencies in such modulated structures. This is because a current source in the hot emitter at frequency ω generates photons that cross the vacuum gap and generate sideband photons at $\omega + n\Omega$, which in turn experience partial reflection back into the vacuum gap, resulting in negative Poynting flux at the sideband frequencies.

By integrating the spectral heat flux in Fig. 3(b), we obtain $\Delta P = +282.2$ mW/m^2, indicating that heat flows against the temperature gradient. Further, we obtain a total work input of $\dot{W} = 129$ mW/m^2, resulting in a COP of $(\Delta P/\dot{W}) - 1 = 1.188$. Therefore, the structure shown in Fig. 2(a) indeed achieves photonic refrigeration after integration over all frequencies and wavevectors. In Fig. 3(c), we plot the COP obtained from this system as a function of the modulation strength δ. The system begins to exhibit cooling for $\delta > 0.3$, reaching a COP of around 1.4 for large modulation strengths. The performance of the full system is below the single-channel case of Fig. 2 because the modes in the photonic crystal have varying frequency separations and linewidths as

the wavevectors (channels) are varied, as shown in Fig. 3(d). Due to this mismatch between the modulation frequency and the modal frequency separation, not all channels contribute equally to the cooling. Further improvements to the performance are possible, for example, by engineering the modal frequency separation to be constant over a larger angular range or reducing the gap distance between the hot and cold sides to the near field regime.

We end the paper by briefly discussing our work in the context of existing photon-based active cooling approaches, i.e., laser cooling and electroluminescent cooling. The mechanism of laser cooling [24–26] is based on an anti-Stokes luminescence up-conversion process [27]. However, the COP of laser cooling is inherently limited to be several orders of magnitude below the Carnot bound due to the small energy difference between the luminescence photon and the pump photon [28]. Alternatively, electroluminescent cooling has been suggested to realize photonic cooling [29–34]. However, positive electroluminescent cooling has not been demonstrated to date due to the stringent requirements on the luminescence efficiency, while negative electroluminescent cooling [34] suffers from low power density. In comparison, the mechanism of modulation-induced cooling discussed here can exhibit a much larger COP than laser cooling, and being based on thermal radiation, can potentially overcome the stringent luminescence efficiency requirements in laser- and electroluminescent-cooling.

---

* sbuddhi@stanford.edu, shanhui@stanford.edu

[1] S. Fan, Joule **1**, 264 (2017).

[2] W. Li and S. Fan, Optics Express **26**, 15995 (2018).

[3] A. Lenert, D. M. Bierman, Y. Nam, W. R. Chan, I. Celanović, M. Soljačić, and E. N. Wang, Nature Nanotechnology **9**, 126 (2014).

[4] A. P. Raman, M. A. Anoma, L. Zhu, E. Rephaeli, and S. Fan, Nature **515**, 540 (2014).

[5] O. Ilic, P. Bermel, G. Chen, J. D. Joannopoulos, I. Celanovic, and M. Soljačić, Nature Nanotechnology **11**, 320 (2016).

[6] J.-J. Greffet, R. Carminati, K. Joulain, J.-P. Mulet, S. Mainguy, and Y. Chen, Nature **416**, 61 (2002).

[7] X. Liu, T. Tyler, T. Starr, A. F. Starr, N. M. Jokerst, and W. J. Padilla, Physical Review Letters **107**, 045901 (2011).

[8] C. Khandekar, A. Pick, S. G. Johnson, and A. W. Rodriguez, Physical Review B **91**, 115406 (2015).

[9] I. Latella, R. Messina, J. M. Rubi, and P. Ben-Abdallah, Physical review letters **121**, 023903 (2018).

[10] Z. Yu and S. Fan, Nature Photonics **3**, 91 (2009).

[11] K. Fang, Z. Yu, and S. Fan, Physical Review Letters **108**, 153901 (2012).

[12] D. L. Sounas and A. Alù, Nature Photonics **11**, 774 (2017).

[13] Y. Hadad, J. C. Soric, and A. Alu, Proceedings of the National Academy of Sciences **113**, 3471 (2016).

[14] C. R. Otey, W. T. Lau, and S. Fan, Physical Review Letters **104**, 154301 (2010).

[15] L. Zhu, S. Sandhu, C. Otey, S. Fan, M. B. Sinclair, and T. S. Luk, Applied Physics Letters **102**, 103104 (2013).

[16] H. Iizuka and S. Fan, Physical Review Letters **120**, 063901 (2018).

[17] D. Polder and M. Van Hove, Physical Review B **4**, 3303 (1971).

[18] K. Chen, B. Zhao, and S. Fan, Computer Physics Communications **231**, 163 (2018).

[19] D. Whittaker and I. Culshaw, Physical Review B **60**, 2610 (1999).

[20] S. Inampudi, M. M. Salary, S. Jafar-Zanjani, and H. Mosallaei, Optical Materials Express **9**, 162 (2019).

[21] C. H. Henry and R. F. Kazarinov, Reviews of Modern Physics **68**, 801 (1996).

[22] C. Khandekar, R. Messina, and A. W. Rodriguez, AIP Advances **8**, 055029 (2018).

[23] Y. Shi, Q. Lin, M. Minkov, and S. Fan, IEEE Journal of Selected Topics in Quantum Electronics **24**, 1 (2018).

[24] R. I. Epstein, M. I. Buchwald, B. C. Edwards, T. R. Gosnell, and C. E. Mungan, Nature **377**, 500 (1995).

[25] D. V. Seletskiy, S. D. Melgaard, S. Bigotta, A. Di Lieto, M. Tonelli, and M. Sheik-Bahae, Nature Photonics **4**, 161 (2010).

[26] J. Zhang, D. Li, R. Chen, and Q. Xiong, Nature **493**, 504 (2013).

[27] P. Pringsheim, Zeitschrift für Physik **57**, 739 (1929).

[28] D. V. Seletskiy, R. Epstein, and M. Sheik-Bahae, Reports on Progress in Physics **79**, 096401 (2016).

[29] J. Tauc, Cechoslovackij Fiziceskij Zurnal **7**, 275 (1957).

[30] P. Berdahl, Journal of Applied Physics **58**, 1369 (1985).

[31] K. Chen, P. Santhanam, S. Sandhu, L. Zhu, and S. Fan, Physical Review B **91**, 134301 (2015).

[32] K. Chen, P. Santhanam, and S. Fan, Physical Review Applied **6**, 024014 (2016).

[33] T. P. Xiao, K. Chen, P. Santhanam, S. Fan, and E. Yablonovitch, Journal of Applied Physics **123**, 173104 (2018).

[34] L. Zhu, A. Fiorino, D. Thompson, R. Mittapally, E. Meyhofer, and P. Reddy, Nature **566**, 239 (2019).